VOL. 11, NO. 1, JANUARY 2016 ISSN 1819-6608
ARPN Journal of Engineering and Applied Sciences

www.arpnjournals.com

A CRITICAL ASSESSMENT ON EVAPORATIVE COOLING PERFORMANCE OF MICRO FINNED MICRO GAP FOR HIGH HEAT FLUX APPLICATIONS

Shugata Ahmed[1], Ahmad Faris Ismail[1], Erwin Sulaeman[1] and Muhammad Hasibul Hasan[2]
[1]Departmental of Mechanical Engineering, Faculty of Engineering, Jalan Gombak, Kuala Lumpur, Malaysia
[2]Departmental of Manufacturing and Materials Engineering, Faculty of Engineering, Jalan Gombak, Kuala Lumpur, Malaysia
Mail: shugataahmed@gmail.com

ABSTRACT

Micro gap heat sinks reduce flow boiling instabilities and generate more uniform surface temperature than typical microchannels. Heat transfer rate in micro gaps can be increased by providing micro fins. Micro fins increase surface area as well as generate turbulence, which disturbs the laminar sub-layer. Hence, heat transfer rate enhances due to rapid fluid mixing. In this paper, effectiveness of flow boiling in a micro finned micro gap for cooling purpose has been investigated numerically. Flow boiling of pure water in the heat sink has been simulated using FLUENT 14.5 release. From results, it has been observed that upper and lower solid-fluid interfaces show different thermal behaviors with heat flux increment. Area-weighted average heat transfer coefficient of upper surface increases with increasing heat flux, while decreases for lower surface. In a net effect, thermal resistance of the heat sink increases with heat flux increment after onset of boiling for low Reynolds number. However, for high Reynolds number, thermal resistance changes slowly with heat flux variation. Pressure drop penalty has been found high for high heat fluxes during boiling. Interestingly, increment of pumping power is not always cost effective as thermal resistance does not decrease sharply all over the range. Hence, it is suggested that optimized pumping power should be used for highest efficiency.

Keywords: micro fin, micro gap, flow boiling, thermal resistance and pumping power.

INTRODUCTION

Microchannel heat sinks are widely used for thermal management of microelectronic devices, microelectromechanical systems (MEMS), photovoltaic cells, solar collectors and fuel cells. Due to high surface-to-volume ratio, heat transfer rate is high in microchannels. In 1981, the concept was first developed by Tuckerman and Peace [1] for cooling of very large scale integrated (VLSI) circuits. They discovered that heat transfer rate from a 60 μm wide and 302 μm deep channel is up to 790 $\mathrm{Wm^{-2}}$ and pressure drop is 2 bar for water coolant. High pumping power is required to drive the fluid as pressure drop is high in microchannels.

Recently, it has been found that micro gaps have advantages over microchannels for two-phase flow. In micro gaps, walls of microchannels, which act as fins, are eliminated and coolant flows through the gap. The significant beneficial characteristics of micro gaps over microchannels are generation of more uniform surface temperature, decrement of flow boiling instability, lower pressure drop and high heat transfer coefficient [2]. In engineering, high heat flux applications are common in high performance computers, reactors; laser diodes etc. [3] Effective cooling system is required for thermal management of these devices. Micro gap heat sink may possess the capability of efficient cooling for high heat flux applications. Hence, thermal and hydrodynamic behaviour of this potential heat sink for high heat flux should be studied.

Alam *et al*. [4] investigated heat transfer and pressure drop characteristics of three different micro gaps of190 μm, 285 μm and 381 μm heights. Experimental results showed that heat transfer coefficient increases with the decrement of gap size. On the other hand, pressure drop is higher for smaller gap sizes. However, in another publication, Alam *et al.* [5] stated that below100 μm, dry out takes place very early. Hence, it is not suitable for cooling purpose. They showed that the gap size should be between $100 - 500$ μm for effective cooling.

Micro fins are used in a structure to increase heat transfer surface area. Stehlík *et al*. [6] commented that fins also generate turbulence. Hence, heat transfer coefficient increases in micro finned structures. Micro fins can be effectively used with micro gap heat sinks for high performance cooling. In Figure-1, a micro finned micro gap heat sink created by ANSYS Workbench Design Modeler has been shown.

The heat transfer phenomenon of heat sinks with micro pin fins has been explored experimentally by Liu *et al.* [7]. They showed that micro finned heat sinks posses high heat transfer capability. According to them, thermal resistance of the heat sink decreases with increasing pressure drop. Shafeie *et al*. [8] also studied the effect of micro pin fins on microchannels. Their results showed that micro pin finned structures perform slightly better than optimized conventional microchannel heat sink for small pumping power. Flow boiling in a micro finned structure is also found highly efficient for cooling, although pressure drop penalty is higher than smooth surfaces.

Chang *et al.* [9] showed that two phase heat transfer coefficient increases effectively by adding micro pin fins on silicon chip. Li *et al.* [10] also observed that two phase heat transfer coefficient increases 40 - 120 % in 3D micro finned tube in comparison to smooth tube. However, pressure drop was also found higher in micro finned tube than smooth one. Pressure drop and heat transfer characteristics of subcooled and nucleate boiling of water in a micro pin finned structure was investigated by McNeil *et al.* [11].

In this paper, flow boiling of pure water in micro finned micro gap has been simulated using FLUENT 14.5 release. The purpose of this study is to find out related conditions that should be maintained to enhance efficiency of the heat sink for high heat flux applications. Effects of heat flux on heat transfer coefficient and thermal resistance have been investigated for both laminar and turbulent flow. Heat transfer effect on pressure drop has also been observed. In addition, significance of pumping power on heat transfer characteristics of micro finned micro gap has been explored.

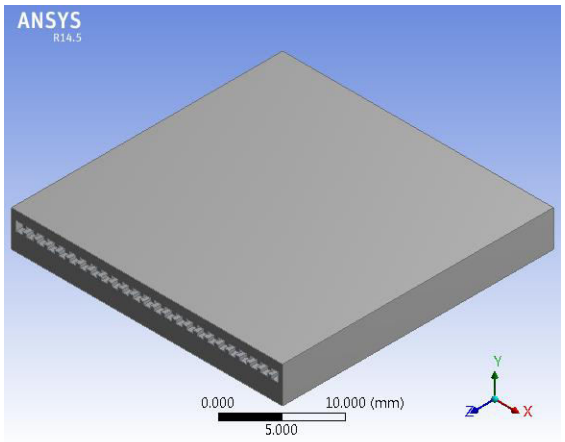

Figure-1. Micro finned micro gap (3D view).

MATHEMATICAL MODEL

Governing equations

A complete mathematical model of the system is necessary for numerical analysis of the heat sink. Volume of Fluid (VOF) model has been used for multiphase flow modeling [12]. In VOF model, each phase is considered as a single-fluid. Hence, separate sets of governing equations are used for liquid and vapor phases. Steady-state governing equations of flow boiling are provided, which have been solved numerically by applying proper boundary conditions. Details of CFD analysis has been followed from publication of Kelvin *et al.* [13]

The continuity equation for vapor phase, which is also known as void fraction equation, is the following:

$$\rho_v \nabla(\alpha.\vec{\boldsymbol{v}}_v) = \dot{m}_{l\to v} - \dot{m}_{v\to l} \quad (1)$$

Here ρ_v and $\vec{v}_v$ are density and velocity of vapor respectively. By solving Eqn. (1), distribution of void fraction α is obtained in the flow domain. Later volume fraction distribution of liquid phase is calculated from $1-\alpha$. $\dot{m}_{l\to v}$ and $\dot{m}_{v\to l}$ represent mass transfer from liquid to vapor and vice versa respectively.

For a Newtonian fluid, conservation of momentum equation is given below:

$$\rho\nabla(\vec{\boldsymbol{v}}.\vec{\boldsymbol{v}}) = -\nabla P + \nabla\tau + \rho\vec{\boldsymbol{g}} + \vec{\boldsymbol{F}}_{\boldsymbol{\sigma}} \quad (2)$$

In Eqn. (2), ∇P and $\nabla\tau$ are pressure and shear stress gradients respectively, $\vec{\boldsymbol{g}}$ is the gravitational acceleration and $\vec{\boldsymbol{F}}_{\boldsymbol{\sigma}}$ denotes the surface tension force.

Conservation of energy equation for fluid domain is written as:

$$\rho_v\nabla(\alpha.E_v.\vec{\boldsymbol{v}}_v) = \nabla\left(k_{eff}\nabla\theta_v\right) + h_{lv}(\dot{m}_{v\to l} - \dot{m}_{l\to v}) \quad (3)$$

Here E_v and θ_v are enthalpy and temperature of vapor respectively, k_{eff} represents effective thermal conductivity and h_{lv} is the enthalpy of vaporization.

For solid domain, the energy equation can be written as:

$$\nabla(k_s\nabla\theta) = 0 \quad (4)$$

Here $C_{p,s}$ and θ are specific heat capacity and temperature of the solid domain respectively.

Mass exchange between two phases is calculated from evaporation-condensation model, proposed by Lee [14].

$$\dot{m}_{l\to v} = \varepsilon * (1-\alpha)\rho_l\frac{(T_l - T_{sat})}{T_{sat}} \quad (5)$$

$$\dot{m}_{v\to l} = \upsilon * \alpha\rho_v\frac{(T_{sat} - T_v)}{T_{sat}} \quad (6)$$

Here, ε and υ are evaporation and condensation coefficients respectively. Wu *et al.* [15], De Schepper *et al.* [16] and Alizadehdakhel *et al.* [17] recommended the value 0.1 of these coefficients to maintain interfacial temperature close to saturation temperature, T_{sat}.

Renormalization Group Theory (RNG) based $k-\varepsilon$ turbulence model [18] has been used to simulate the turbulent flow. Governing equations for turbulence are given below:

$$\rho\nabla(\vec{\boldsymbol{v}}.k) = \nabla\left(a_k.\mu_{eff}.\nabla k\right) + G_k + G_b - \rho\varepsilon - Y_M + S_k \quad (7)$$

$$\rho\nabla(\vec{\boldsymbol{v}}.\varepsilon) = \nabla\left(a_\varepsilon.\mu_{eff}.\nabla\varepsilon\right) + C_{1\varepsilon}\frac{\varepsilon}{k}(G_k + C_{3\varepsilon}G_b) - C_{2\varepsilon}\rho\frac{\varepsilon^2}{k} - R_\varepsilon + S_\varepsilon \quad (8)$$

In above equations, k and ε are turbulent kinetic energy and rate of energy dissipation respectively.

G_k = generation of turbulent kinetic energy due to the mean velocity gradients.

G_b = generation of turbulent kinetic energy due to buoyancy.

Y_M = contribution of the fluctuating dilatation in compressible turbulence to the overall dissipation rate.

a_k and a_ε are inverse effective Prandtl numbers for k and ε respectively and S_k and S_ε are source terms.

The model constants have following default values:

$C_{1\varepsilon}$ = 1.42, $C_{2\varepsilon}$ = 1.68

Reynolds number is defined as:

$$Re = \frac{\rho v D_h}{\mu} \tag{9}$$

Here, D_h is the hydraulic diameter of the heat sink and μ is the dynamic viscosity of the fluid.

Total thermal resistance is the summation of conductive and convective thermal resistance, which is obtained from following equation:

$$R_{th} = R_{cond} + R_{conv} = \frac{H}{k_s A_s} + \frac{1}{h A_f} \tag{10}$$

A_s and A_f represent available area of heat transfer in solid and fluid respectively.

Again, pumping power:

$$\Omega = v A_c \Delta P \tag{11}$$

Here, A_c is the cross-sectional area and ΔP represents pressure drop.

Boundary conditions

Following boundary conditions are applied in the computational domain:

Inlet: $T_f = T_{in}$, $\dot{m} = \dot{m}_{in}$, $\alpha = 0$. In this study, inlet temperature of water has been kept constant at 25℃.

Outlet: $P = P_{out}$. Atmospheric pressure is defined at the outlet of the heat sink.

Solid-fluid interface: Heat transfer from wall to fluid by convection, $q_{eff} = h(\theta - \theta_f)$.

Channel bottom wall: Uniform heat flux is applied at the bottom of the heat sink. Heat is transferred through solid wall by conduction in the normal direction of bottom surface, $q = -k_s \frac{\partial \theta}{\partial n}$.

Other channel walls: Other channel walls are considered as insulated. Hence, $\frac{\partial \theta}{\partial n} = 0$.

GEOMETRY, MESHING AND NUMERICAL SOLUTION

The geometry has been generated by ANSYS Workbench Design Modeler. Dimensions of the sink are provided in Table-1. Heat sink material is aluminum. After creating geometry, fine meshing has been done. Number of meshing elements has been optimized to reduce computational time. The mesh used in the simulation consists of 3633747 numbers of elements. Fluid flow and heat transfer are assumed as steady-state.

FLUENT uses Finite Volume Method to solve governing equations. Second Order Upwind scheme has been used for spatial discretization of the governing equations. Semi-Implicit Method for Pressure Linked Equations (SIMPLE) algorithm, developed by Patankar and Spalding [19] has been adopted to solve pressure-velocity coupling equation.

Table-1. Dimensions of heat sink, micro gap and fins

Parameters (unit)	**Value**
Heat sink height, H (mm)	4
Heat sink width, W (mm)	30
Heat sink length, L (mm)	30
Micro gap height (mm)	1
Fin height, H_{fin} (mm)	0.3
Fin width, W_{fin} (mm)	0.5
Number of fins, N	48

RESULTS AND DISCUSSIONS

Effect of heat flux

In Figure-2, area-weighted average heat transfer coefficient, h of upper and lower surfaces have been plotted for heat flux variation, while Reynolds number has been kept constant at 700. It is perceived that heat transfer coefficient of lower surface decreases rapidly after onset of boiling at 4×10^6 Wm^{-2} heat flux. However, at the same time, heat transfer coefficient of upper surface increases slightly when boiling starts. As decrement rate of h for lower interface is much higher than the increment rate for upper surface, total thermal resistance of the heat sink increases with heat flux increment during boiling, which is observed in Figure-3(a). However, from Figure-3(b), it is seen that for$Re = 3000$, thermal resistance is almost invariant for heat flux variation from $6 \times 10^6 - 11 \times 10^6$ Wm^{-2}and only slightly increases for12×10^6 Wm^{-2}although boiling starts at8×10^6Wm^{-2}. In turbulent flow, evaporation rate is sufficiently small at the beginning of boiling to create any difference from single-phase flow. Void fraction distribution at the lower interface for $Re = 700$ and $Re = 3000$ have been shown by contour plot in Figure-4. It shows that outlet void fraction for $Re = 700$ is 0.35, while for$Re = 3000$, it is

only 0.005 although applied heat flux is same. Moreover, mass transfer rate changes slowly with increasing heat flux. As a result, effect of heat flux variation on thermal resistance is not noticeable.

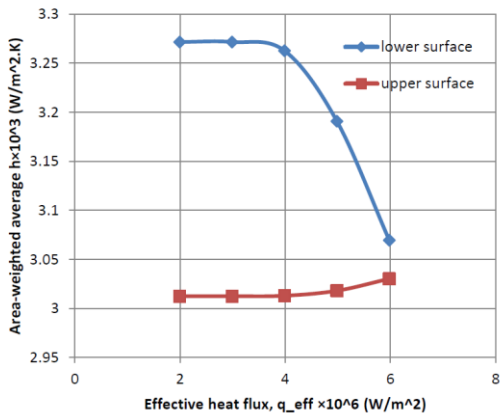

Figure-2. Area-weighted average heat transfer coefficient vs. effective heat flux for$\mathrm{Re} = 700$.

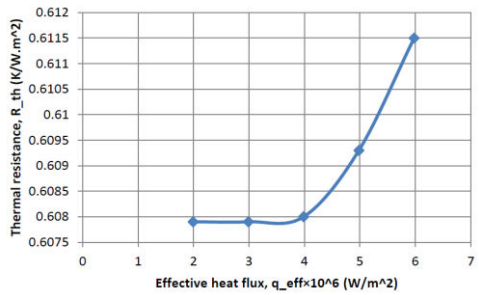

(a)

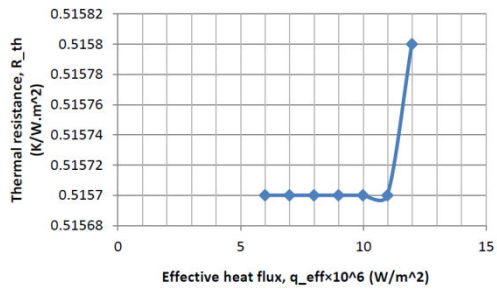

(b)

Figure-3. Thermal resistance vs. effective heat flux for $\mathrm{Re} = 700$ (a) and $\mathrm{Re} = 3000$ (b).

In Figure-5, pressure drop in the micro gap has been plotted for different heat fluxes. It is perceived that pressure drop increases almost linearly with heat flux increment after onset of boiling. For higher heat fluxes, bubble generation is high. These bubbles are pushed to the flow direction by flowing fluid, which causes higher pressure drop.

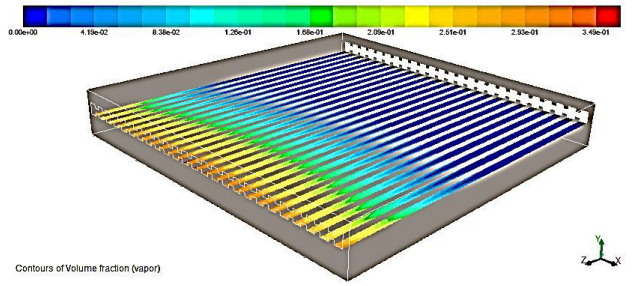

(a)

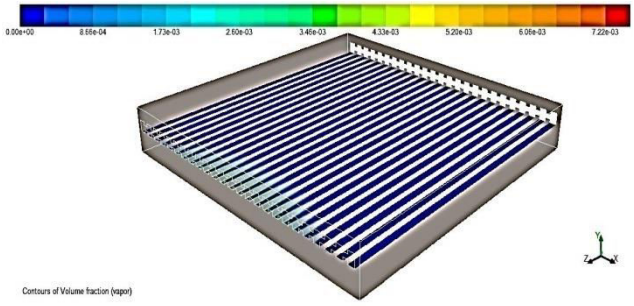

(b)

Figure-4. Void fraction distribution on X-Z plan at Y=2 mm for $\mathrm{Re} = 700$ (a) and $\mathrm{Re} = 3000$ (b), while applied heat flux is $8 \times 10^6\ \mathrm{Wm}^{-2}$

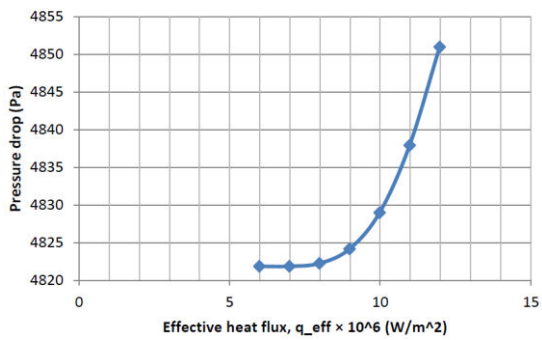

Figure-5. Pressure drop vs. effective heat flux for $\mathrm{Re} = 3000$.

Effect of pumping power

In previous section, it has been discussed that the heat sink should be operated with high Reynolds number for high heat flux applications as increment of thermal resistance is small. However, to obtain high Reynolds number, pumping power needs to increase, which involves cost. Hence, it is necessary to study the effect of pumping power on thermal resistance for constant heat flux.

In Figure-6, thermal resistance has been plotted for various pumping powers, while heat flux is kept constant at $6 \times 10^6\ \mathrm{Wm}^{-2}$. It is observed that decrement rate of thermal resistance, $\mathrm{R_{th}}$ is not constant for total range of pumping power,Ω

First,$\mathrm{R_{th}}$ decreases sharply with pumping power increment. However, after exceeding$\Omega = 0.008\ \mathrm{W}$, decrement rate of $\mathrm{R_{th}}$ becomes very slow. As a result,

further increment of pumping power after 0.008 W is not cost effective. This phenomenon was also observed by Hung et al. [20] for single-phase flow of water in double-layer microchannel. Manaf *et al*. [21] also showed that decrement rate of thermal resistance is high for low Reynolds numbers in a triangular double-layer microcahnnel heat sink.

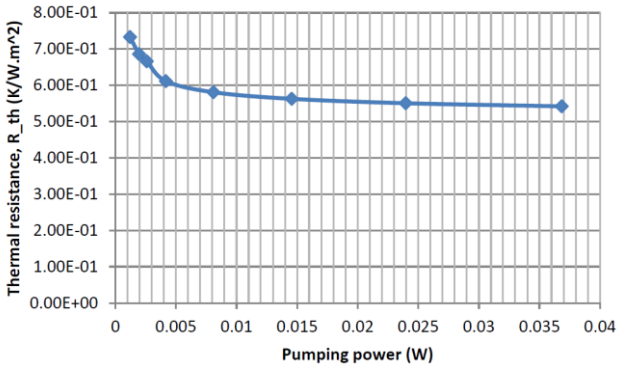

Figure-6. Thermal resistance vs. pumping power for $q_{eff} = 6 \times 10^6\ Wm^{-2}$.

CONCLUSIONS

Thermal and hydraulic characteristics of a micro finned micro gap with high heat fluxes have been studied. It has been found that dependency of various parameters on heat flux is influenced by Reynolds number. Low Reynolds number is responsible for thermal resistance increment with increasing heat flux after onset of boiling. Hence, for high heat flux applications, where evaporation is involved, high Reynolds number should be maintained. During flow boiling, pressure drop increases with heat flux increment. Thermal resistance also depends on pumping power. Decrement rate of thermal resistance with pumping power increment is high only up to a certain range. After that thermal resistance decreases very slowly for further pumping power increment. Hence, pumping power should be optimized.

In this study, only steady-state analysis has been performed. However, a transient solver may provide more accurate simulation data as fluctuation of temperature and pressure drop with time are involved in flow boiling.

ACKNOWLEDGEMENT

The support of the Ministry of Education, Malaysia under the grant FRGS 13-020-0261 is gratefully acknowledged. This research was also supported by International Islamic University Malaysia from Endowment Type B fund (EDW B14-127-1012).

REFERECES

[1] Tuckerman B. and Pease R. F. W. 1981. High-performance heat sinking for VLSI. Electron Device Letters, IEEE 2.5. 126-129.

[2] Alam T., Lee P. S., Yap C. R. and Jin L. W. 2011. Experimental investigation of microgap cooling technology for minimizing temperature gradient and mitigating hotspots in electronic devices. 13th Electronics Packaging Technology Conference (EPTC). pp. 530-535.

[3] Kandlikar S. G. 2005. High flux heat removal with microchannels - a roadmap of challenges and opportunities. Heat Transfer Engineering. 26(8): 5-14.

[4] Alam T., Lee P. S., Yap C. R. and Jin L. W. 2012. Experimental investigation of local flow boiling heat transfer and pressure drop characteristics in microgap channel. International Journal of Multiphase Flow. 42: 164-174.

[5] Alam T., Lee P. S., Yap C. R., Jin L. W. and Balasubramanian K. 2012. Experimental investigation and flow visualization to determine the optimum dimension range of microgap heat sinks. International Journal of Heat and Mass Transfer. 55(25): 7623-7634.

[6] Stehlík P., Jegla Z. and Kilkovský B. 2014. Possibilities of intensifying heat transfer through finned surfaces in heat exchangers for high temperature applications. Applied Thermal Engineering. 70(2): 1283-1287.

[7] Liu M., Liu D., Xu S. and Chen Y. 2011. Experimental study on liquid flow and heat transfer in micro square pin fin heat sink. International Journal of Heat and Mass Transfer. 54(25): 5602-5611.

[8] Shafeie H., Abouali O., Jafarpur K. and Ahmadi G. 2013. Numerical study of heat transfer performance of single-phase heat sinks with micro pin-fin structures. Applied Thermal Engineering. 58(1): 68-76.

[9] Chang W. R., Chen C. A., Ke J. H. and Lin T. F. 2010. Subcooled flow boiling heat transfer and associated bubble characteristics of FC-72 on a heated micro-pin-finned silicon chip. International Journal of Heat and Mass Transfer. 53(23): 5605-5621.

[10] Li L., Cui W., Liao Q., Mingdao X., Jen T. C. and Chen Q. 2005. Heat transfer augmentation in 3D internally finned and microfinned helical tube. International journal of heat and mass transfer. 48(10): 1916-1925.

[11] McNeil D. A., Raeisi A. H., Kew P. A. and Hamed, R. S. 2014. An investigation into flow boiling heat transfer and pressure drop in a pin–finned heat sink. International Journal of Multiphase Flow. 67: 65-84.

[12] Hirt C. W. and Nichols B. D. 1981. Volume of fluid (VOF) method for the dynamics of free boundaries. Journal of Computational Physics. 39(1): 201–225.

[13] Kelvin H.C.S., Yousif A.A. and Andrew C. 2012. Unsteady heat transfer in an annular pipe, Part II: swirling laminar flow. IIUM Engineering Journal. 12(6): 79-95.

[14] Lee W. H. (1979). A Pressure Iteration Scheme for Two-Phase Modeling, Technical Report LA-UR. Los Alamos Scientific Laboratory, Los Alamos, New Mexico. pp. 79-975.

[15] Wu H. L., Peng X. F., Ye P. and Gong Y. E. 2007. Simulation of Refrigerant Flow Boiling in Serpentine Tubes. International Journal of Heat and Mass Transfer. 50(5): 1186-1195.

[16] De Schepper, S. C., Heynderickx G. J. and Marin G. B. 2009. Modeling the Evaporation of a Hydrocarbon Feedstock in the Convection Section of a Steam Cracker. Computers and Chemical Engineering. 33(1): 122–132.

[17] Alizadehdakhel A., Rahimi M. and Alsairafi A. A. 2010. CFD Modeling of Flow and Heat Transfer in a Thermosyphon. International Communications in Heat and Mass Transfer. 37(3): 312–318.

[18] Orszag S. A., Yakhot V., Flannery W. S., Boysan F., Choudhury D., Maruzewski J. and Patel B. 1993. Renormalization Group Modeling and Turbulence Simulations. International Conference on Near-Wall Turbulent Flows, Tempe, Arizona. pp. 1031-1046.

[19] Patankar S. V. and Spalding, D. B. 1972. A calculation procedure for heat, mass and momentum transfer in three-dimensional parabolic flows. International Journal of Heat and Mass Transfer. 15(10): 1787-1806.

[20] Hung T. C. and Yan W. M. 2012. Enhancement of thermal performance in double-layered microchannel heat sink with nanofluids. International Journal of Heat and Mass Transfer. 55(11): 3225-3238.

[21] Manaf H., Ahmed S., Ahmed M. I., and Hawlader M. N. A. 2014. A triangular double layer microchannel heat sink: effect of parallel and counter flow. Advanced Materials Research, Advances In Manufacturing And Materials Engineering. pp. 433-439.